On the failure criterion of weak-snow layers using the discrete element method

Johan Gaume[1,*], Guillaume Chambon[2], Ingrid Reiweger[1], Alec van Herwijnen[1], Jürg Schweizer[1]

[1] WSL Institute for Snow and Avalanche Research SLF, Davos, Switzerland

[2] IRSTEA, Grenoble, France

ABSTRACT: The release of dry-snow slab avalanches start with a local failure in a weak snow layer underlying a cohesive slab followed by crack propagation within the weak layer. Our knowledge of these processes is limited by the complex microstructure of snow. It is not clear how to characterize the mechanical behavior of weak snowpack layers under mixed-mode loading. While most current studies assume pure shear or Mohr-Coulomb failure criterions, which may apply for non-persistent weak layers or weak interfaces, such a failure criterion does not account for the collapsible nature of some weak snowpack layers. To clarify this issue, we use the discrete element (DE) method to investigate the failure criterion of different types of weak layers. As the DE model mimics the high porosity of snow, the collapse of the structure in the weak layer during fracture can be studied. Simple shear loading simulations were carried out for different slope angles which enabled to highlight a new mixed-mode shear-compression failure envelope. Simulations of propagation saw tests (PST) were performed to analyze the influence of weak layer collapse and the mechanical properties of the slab on the critical length required for the onset of crack propagation. Finally, a simple analytical model able to accurately reproduce the DE simulations is proposed.

KEYWORDS: Snow avalanche, failure criterion, Mohr-Coulomb, crack propagation, discrete element modeling, snow slab, weak layer.

1 INTRODUCTION

The release of dry-snow slab avalanches is due to the failure of a weak snow layer underlying cohesive snow slab layers. As the load on the snowpack increases, local damage in the weak layer is assumed to develop into a crack which can rapidly propagate if its size exceeds a critical length. These two processes, namely, failure initiation and crack propagation are necessary conditions for avalanche release (McClung, 1979; Schweizer and others, 2003).

Our knowledge of release processes is limited by the complex microstructure of snow and its highly porous character. The structural collapse of the weak layer (WL) observed in some field experiments (van Herwijnen and Jamieson, 2005) or evidenced by "whumpf" sounds has raised the question of the origin of the initial WL failure, whether it is in shear or compression. If we assume that damage in the weak layer is due to

bond breaking at the microscopic scale, the stress distribution at the grain scale will be highly complex and the failure mode still largely unknown. In any case, this question is rather irrelevant since shear and compression failure types seem to be linked.

With regards to avalanche hazard assessment, the knowledge of the failure criterion of weak snow layers is essential. Hence, in analogy with other granular materials like sand and based on field data (Zeidler and Jamieson, 2005; McClung and Schweizer, 2006) the Mohr-Coulomb (MC) theory has been used to describe the failure of weak-snow layers (Chiaia et al., 2009; Gaume et al., 2013; Podolskiy et al., 2014). However, the MC criterion might be suitable to evaluate the release conditions on sufficiently steep slopes, typically more than 30° but it will obviously fail in describing failures on flatter slopes and remote triggering when an additional load is involved.

To shed more light on this issue, we use the discrete element (DE) method to investigate the failure criterion of different types of weak layers. As the high porosity of snow can be accounted for in a DE model, the collapse of the structure in the weak layer during fracture can be studied. Simple shear loading simulations were carried out for different slope angles which enabled to highlight a

Corresponding author address: Johan Gaume, WSL Institute for Snow and Avalanche Research SLF, Flüelastrasse 11, CH-7260 Davos Dorf, Switzrland;

tel: +33 6 748 23 547;

email: gaume@slf.ch

new mixed-mode shear-compression failure envelope. Then, PST simulations were performed to analyze the influence of weak layer collapse and the mechanical properties of the slab on the critical length required for unstable crack propagation. Finally, a simple analytical model able to accurately reproduce the DE simulations is proposed.

2   DATA AND METHODS

2.1 Weak layer failure laboratory experiments

We use laboratory data from experiments performed using a load-controlled shear apparatus (Fig. 1a; Reiweger and Schweizer, 2013). The experiments were carried out with snow samples containing a weak layer consisting of artificially produced faceted crystals. The samples were loaded until fracture under different loading rates and at various tilt angles (Fig. 1b). For the sake of the numerical-experimental comparison, we only retained a subset of the data with the fastest loading rates since sintering effects, which might change the failure behavior for low loading rates, were not accounted for in our model.
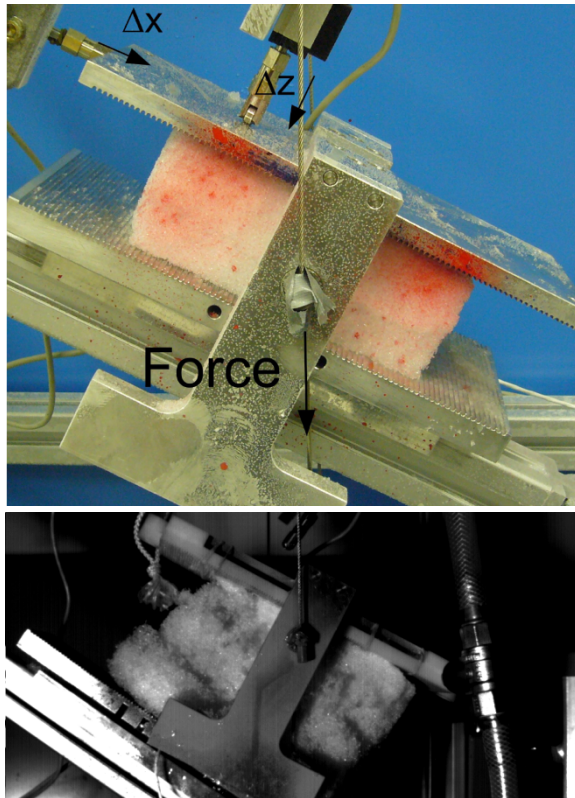

Fig. 1. (a) Snow sample in the shear loading apparatus. (b) Catastrophic failure. From Reiweger and Schweizer (2013).

2.2 Discrete element model

2.2.1 Motivation and objectives

Discrete element (DE) modelling (Cundall and Stark, 1979) allows computing the motion of a large number of small particles by solving dynamic equations for each particle and assuming a contact law between them. Furthermore, at each material point within the sample the DE method allows assessing mechanical quantities such as stress, displacement, deformation rate, porosity, etc. Experimentally, this would be an impossible task. Hence, using DE, the mechanical and rheological behavior of the material can be explored locally, regardless of the spatial heterogeneities possibly displayed by the structure of the material and its mechanical quantities. This method can thus help to better understand physical processes at play in granular-like assemblies.

The DE method has widely been used to study the flow of granular materials for industrial (e.g. Chauduri et al., 2006; Sarkar et al., 2010) or environmental applications such as snow dynamics (e.g. Rognon et al., 2008; Faug et al., 2009) or to model the failure behavior of cohesionless (e.g. Nicot et al., 2004) or cohesive granular materials (e.g. van Baar, 1996; Delenne et al., 2004; Thakur et al., 2014). However, to our knowledge, the DE method has never been used to model the failure in very porous cohesive granular assemblies such as weak-snow layers.

2.2.2 Formulation of the model: loading tests

Simulated systems

The DE simulations were performed using the commercial software PFC2D (by Itasca), which implements the original soft-contact algorithm described in Cundall and Strack (1979). The simulated systems (Fig. 2) are two-dimensional and are composed of a completely rigid basal layer, a WL of thickness h_{wl} and a slab of thickness D = 0.2 m. The slab is composed of grains of radius r = 0.01 m with a primitive cubic packing (or isometric). The porosity of the slab is equal to 21%. Hence the density of the slab ρ can be adjusted by changing the particle density ρ_p (varied in the simulations). The WL is composed of grains of radius r_{wl} = $r/2$. Different types of WL were modeled. The two first types of WL (#1: Fig. 2a and #2: Fig. 2b) are made of collapsible triangular forms, roughly representing the porous structure of persistent WLs such as surface hoar or depth hoar. The difference between the two types consists not only in a different thickness (#1: h_{wl} = 3 mm; #2:

h_{wl} = 4.5 mm) but also in a different structure angle. The half angle on top of the triangle is equal to 40° in case #1 and to 30° in case #2. The last type of WL (#3: Fig. 2c) is more complex, more similar to a weak layer consisting for instance small facetted grains, and was generated by random cohesive pluviation. This means that the grains were randomly distributed inside the space above the rigid base and submitted to gravity. Each new contact during the grains free fall resulted in a permanent contact so as to obtain a sufficient porosity to represent a WL. Note that the numerical grains are not intended to represent the real snow grains which are obviously smaller and whose size is generally larger for the WL.
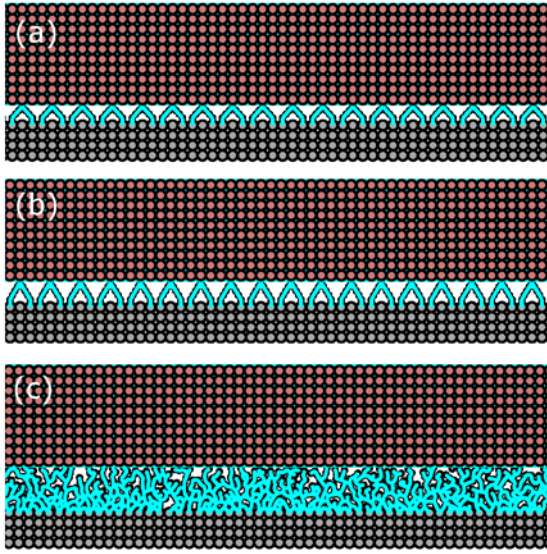

Fig. 2. Systems simulated using the discrete element method subjected to mixed-mode shear-compression loading. (a) case #1, (b) case #2 and (c) case #3.

Contact law
We used the same interparticle contact law (including the numerical values of the parameters) as described in Gaume et al. (2014). The cohesive bond model was also the same as in Gaume et al, (2014), however, the numerical values of the parameters were different. The cohesive bond can be envisioned as a point of glue with constant normal and shear stiffness k_n^b and k_s^b acting at the contact points. This bond has a specified tensile and shear strength σ_t and σ_s. The maximum tensile and shear stresses on the bond are calculated via beam theory according to:

$$\sigma_{max} = -\frac{F_n}{A} + \frac{|M|r_{wl}}{I} \qquad (1a)$$

$$\tau_{max} = \frac{|F_s|}{A} \qquad (1b)$$

where F_n and F_s are the bond normal and shear forces, M is the bending moment, $A = \pi r_{wl}^2$ and $I = \pi r_{wl}^4/4$. If the maximum tensile stress exceeds the normal strength ($\sigma_{max} \geq \sigma_t$), or the maximum shear stress exceeds the shear strength ($\tau_{max} \geq \sigma_s$), then the parallel bond breaks. The parameters used for the bond model of the WL are summarized in Tab. 1. For the mixed-mode loading tests, the slab is considered as a perfectly rigid material.

Tab. 1. Mechanical parameters used in the simulations for the cohesive law. k_n^b: bond normal stiffness; k_s^b: bond shear stiffness; σ_t: bond tensile strength; σ_s: bond shear strength.

	k_n^b (Pa/m)	k_n^b/k_s^b	σ_t^b (Pa)	σ_t^b/σ_s^b
WL #1	1×10^{10}	2	4×10^4	2
WL #2	1×10^{10}	2	1.6×10^4	2
WL #3	1×10^{10}	2	8×10^4	2

Loading
Loading is applied by gravity by progressively increasing the density of the slab until catastrophic failure of the system. Simulations were carried out for different loading angles θ corresponding to the orientation of gravity according to $g_x = g \sin\theta$ and $g_z = g \cos\theta$. Hence, pure compression corresponds to $\theta = 0°$, pure shear to $\theta = 90°$ and pure tension to $\theta = 180°$. The failure is identified by analyzing the average velocity of the slab which strongly increases when the WL fails. Note that sub-critical local bond fractures always precede the catastrophic failure and induce temporary fluctuations in the velocity signal which rapidly stabilizes.

2.2.3 Formulation of the model: PSTs

PST simulations were performed to assess the so-called critical length a_c required for the onset crack propagation. The model setup as well as the parameters are described in more detail in a companion paper (Gaume et al., 2014) which addresses the dynamic phase of crack propagation. In this paper, we focus on the onset of crack propagation and the evaluation of the critical length a_c, using a WL of type #2. The main change with regards to the loading tests consists in accounting for slab elasticity. The slab is assumed purely elastic, i.e. tensile failure of the slab is not accounted for (see Gaume et al. 2014 for the influence of slab tensile fracture). Besides, for the

PST simulations, loading is due to the weight of the slab and the translation of a "saw" inside the WL at a constant speed (refer to Gaume et al., 2014 for illustrations). Simulations are carried out for different system parameters, namely different slab densities ρ (varied between 80 and 350 kg/m^3), Young's modulus E of the slab (varied between 1 and 20 MPa) and slope angles θ (varied between 0 and 40°).

3 RESULTS

3.1 Failure envelope

3.1.1 WL types #1 and #2

The shear stress τ versus the normal stress σ_n at the time of catastrophic failure for the two first types of WL is shown in Fig. 3.

For type #1, and for a negative normal stress σ_n (tension), the shear stress increases almost linearly with increasing normal stress. The WL macroscopic tensile strength σ_t, different from the microscopic tensile strength of the bond σ_t^b, is obtained for pure tension ($\theta = 180°$) and is equal to -1.1 kPa. The cohesion (= shear strength at zero normal stress) is equal to 0.7 kPa. Then, for a normal stress larger than approximately 0.2 kPa, the shear stress decreases linearly with increasing normal stress. The compressive strength is found for a pure compression test ($\theta = 0°$) and is equal to 1.2 kPa.
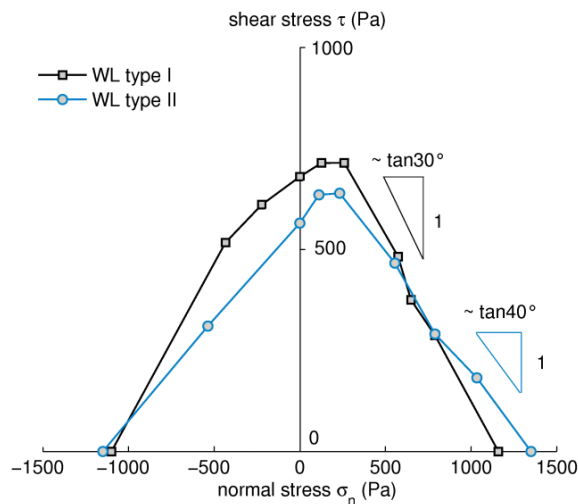

Fig. 3. Failure envelope of WL types #1 and #2 obtained using the DE model and represented in the $\tau - \sigma_n$ (shear vs normal stress) half-plane.

For the second type of WL, the features of the failure envelope are very similar. While the tensile strength and the transition point between increasing and decreasing trends are very similar for both WL types, the cohesion ($c = 0.55$ kPa) and compressive strength ($\sigma_c = 1.35$ kPa) are slightly different. Furthermore, the slope of the increase and decrease of the shear stress with normal stress is closely related to the angle of the structure representing the WL, ~30° for case #1 and ~40° for case #2. This latter result does not depend on the contact friction coefficient μ or on the bond shear strength σ_s^b, indicating that the bonds fail either in tension or due to bending forces (second term in Eq. (1a)) but not in shear. Finally, the tensile strength of the bonds does not influence the form of the failure envelope but only induces a dilatation of the envelope.

3.1.2 WL type #3

Fig. 4 shows the shear stress τ versus the normal stress σ_n at the time of catastrophic failure for the WL of type #3. This WL has a more complex structure than types #1 and #2 and a different failure envelope exhibiting a more "typical" form compared to other granular materials (sand or clay). The shear stress increases as compression increases from approximately 180° to 20°. Then, as the loading angle becomes lower than 20°, the shear stress starts to decrease with increasing normal stress. The tensile strength is equal to -0.36 kPa, the cohesion 0.31 kPa and the compressive strength 3 kPa. The transition between the increasing and decreasing trends of τ with σ_n occurs for a value of σ_n between 2 and 2.5 kPa, much larger than in the two previous cases.

Similarly to the two previous cases, the main determining parameter is the bond tensile strength, which only dilates the failure envelope without influencing its form. This again suggests again that bond failure occurs in tension or due to bending forces. Interestingly, the macroscopic tensile strength is much lower than the bond tensile strength. If we had simulated perfectly straight fibers, the macroscopic tensile strength would be exactly equal to 0.25 times the bond strength since $(r_{wl}/r)^2 = 0.25$ due to the contact orientation. In the present case, the contact bond orientation is randomly distributed and the bonds are therefore more prone to failure since they are subjected to high bending forces [Eq. (1a)]. This also explains why the tensile strength σ_t of WL #2 (1.1 kPa) is closer to its bond tensile strength σ_t^b (16 kPa) than for WL type #1 ($\sigma_t^b = 40$ kPa and

$\sigma_t = 1.1$ kPa). Indeed, for a direct tension test, the contacts are closer to the vertical and thus more prone to fail in tension in case #2 than in case #1; in the latter case bonds support higher bending forces.
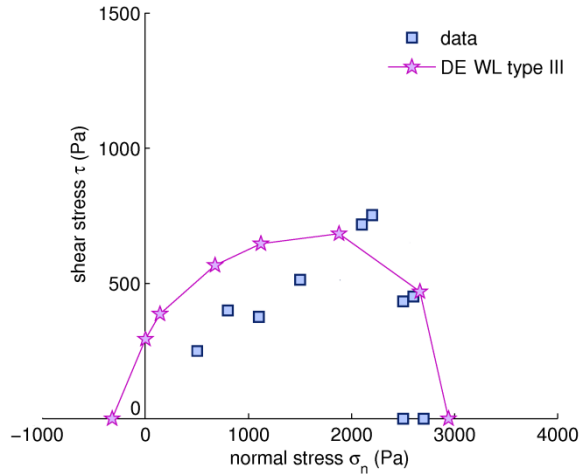

Fig. 4. Failure envelope of WL type #3 and experimental data of failure of faceted crystals (Reiweger and Schweizer, 2013) represented in the $\tau - \sigma_n$ (shear vs normal stress) half-plane.

Finally, we would like to point out that, similarly to what is observed in the laboratory experiments, the WL failure in the simulations is always localized inside the WL along an irregular surface close to the slab-WL interface. Furthermore, WL collapse always constitutes a secondary process of the catastrophic, mixed-mode shear-compression failure.

3.1.3 Experimental results

A subset of the experimental results of the mixed-mode shear-compression loading tests performed by Reiweger and Schweizer (2013) is also shown in Fig. 3. Similarly to the failure envelope of WL type #3, the shear stress at the time of failure increases with increasing normal stress until a certain normal stress threshold after which the shear stress sharply decreases. The compressive strength is equal to ~2.6 kPa and the cohesion and tensile strength were obtained by fitting the subset of the data that increase with σ_n by a classical Mohr-Coulomb line $\tau = c + \sigma_n \tan\varphi$. The cohesion c is equal to ~0.17 kPa, the internal friction angle φ is equal to ~18° and the tensile strength is equal to $-c/\tan\varphi = -0.52$ kPa.

3.2 Influence of the loading angle

Fig. 5 shows the total strength at the time of failure versus the loading angle for the three types of WL as well as the experimental data. The total strength corresponds to the value of $\sqrt{\tau^2 + \sigma_n^2}$ at the time of failure. We first observe that the failure strength for the WL of type #1 hardly depends on the loading angle. For WL type #2, only a slight decrease is observed between 0 and 30°. Indeed, in Fig. 5 loading angles between 0 and 70° are shown, corresponding to only the decreasing part of the failure envelope in Fig. 3 where the total strength does not vary significantly.

For WL type #3, on the other hand, the total strength decreases with increasing slope.
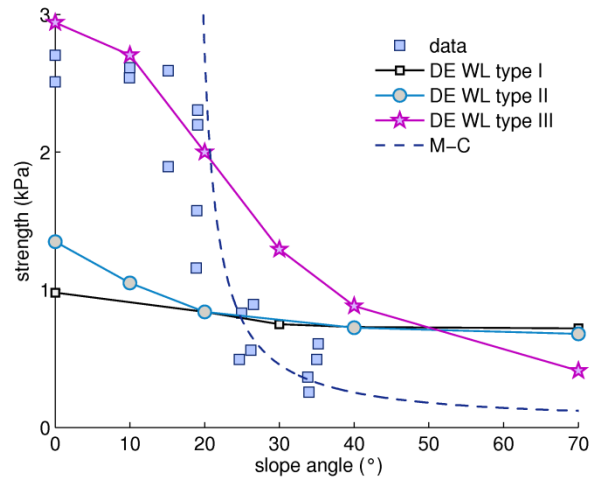

Fig. 5. Total strength as a function of the loading angle for the three types of WL and for experimental data points (Reiweger and Schweizer, 2013). The dashed line is a fit to the data assuming a Mohr-Coulomb criterion with a cohesion c = 0.17 kPa and a friction angle $\varphi = 18°$.

For the experimental data, the decrease is even more pronounced and data for loading angles above the internal friction angle $\varphi = 18°$ are well reproduced by the Mohr-Coulomb criterion.

3.3 Critical length for crack propagation

Different PST simulations were performed for the WL of type #2 for different system parameters. Fig. 6 shows that the critical length a_c increases with increasing Young's modulus of the slab, decreases with increasing slab density and slightly decreases with the slope angle.
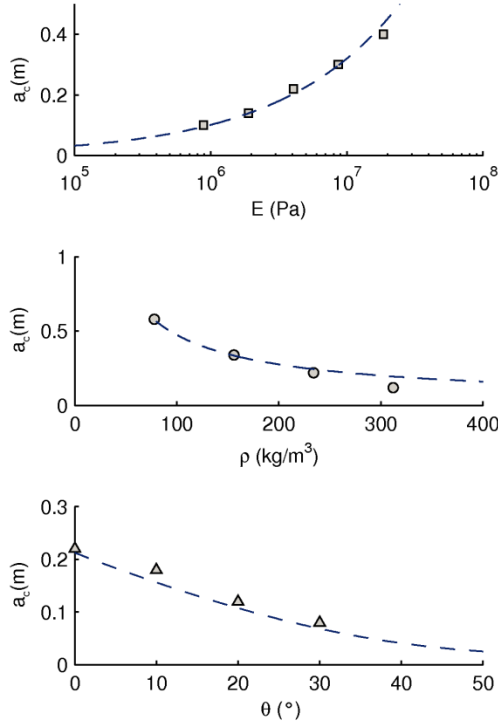
Fig. 6. Critical length a_c for crack propagation inside the WL of type #2 as a function of (a) the slab Young's modulus E for a slab density ρ = 300 kg/m^3, a slab thickness D = 0.2 m and a slope angle θ = 0°. (b) Critical length vs slab density for E = 4 MPa, D = 0.2 m and θ = 0°. (c) Critical length vs slope angle for E = 4 MPa, D = 0.2 m and ρ = 300 kg/m^3. The dashed line represents the modeled critical length according to Eq. (4).

In order to reproduce these trends, an analytical expression was developed. It was shown (Chiaia et al., 2008, Gaume et al., 2013) that the presence of a crack inside the WL induces a stress concentration at the tip of the crack. If slab bending effects are neglected, the maximum stress at the crack tip τ_{max} was found to depend on the shear stress due to the slab τ, the crack length a and the characteristic length of the system Λ according to:

$$\tau_{max} = \tau \left(1 + \frac{a}{\Lambda}\right) \qquad (2)$$

The characteristic length Λ is a function of the effective slab Young's modulus $E' = E/(1 - \square^2)$, with $\square$ the Poisson's ratio of the slab, the slab thickness D, the WL thickness D_{wl} and the WL shear modulus G_{wl}:

$$\Lambda = \sqrt{\frac{E'DD_{wl}}{G_{wl}}} \qquad (3)$$

The problem of Eq. (2) is that the effect of slab bending is not accounted for and thus, there would be no stress concentration for a zero slope angle and consequently no critical length which is clearly contradicted by both field experiments (e.g. van Herwijnen et al., 2010) and the presented simulations (Fig. 6). From our DE simulations, a complete expression of the maximum shear stress at the crack tip was found:

$$\tau_{max} = \tau \left(1 + \frac{a}{\Lambda}\right) + \alpha\sigma_n \left(\frac{a}{\Lambda}\right)^2 \qquad (4)$$

with $\alpha = 0.5$. This expression was confirmed by a finite element analysis of a slab bending over a WL. Note that the bending induced stress (right-term in Eq. (4)) computed using beam theory (Timoshenko and Goodier, 1970) gives a coefficient $\alpha = 3$, and a scaling of a with slab depth D rather than Λ; also, the term according to beam theory would be independent of the slab Young's modulus and largely overestimate the bending stress.

From Eq. (4) the critical length a_c can be easily obtained by solving $\tau_{max} = \tau_p$ where τ_p is the shear stress at the time of failure given by the failure envelope:

$$a_c = \Lambda \left(\frac{-\tau + \sqrt{\tau^2 + 4\alpha\sigma_n(\tau_p - \tau)}}{2\alpha\sigma_n}\right) \qquad (5)$$

This expression is valid for all sets of the system parameters. The modeled critical length was represented on Fig. 6 using for τ_p a linear fit of the failure envelope between 0° and 70° in the Mohr-Coulomb domain. As shown in Fig. 6, the agreement between the modeled critical length and the critical length obtained with DE simulation is excellent.

We also tried to calculate the critical length using the anticrack model of Heierli (2008), but were unable to reproduce the DE results. Indeed, with our approaches (DE and analytical), the critical length is proportional to $\sqrt{E}$ and to ρ^{-1} whereas it is proportional to E and ρ^2 in the anticrack model. This is due to the fact that the anticrack model commonly considers the WL as a perfectly rigid material which is a stringent assumption.

4   DISCUSSION AND CONCLUSIONS

We proposed a novel approach to model WL failure and the onset of crack propagation in a slab-WL system using the cohesive discrete element method with elastic-brittle bonded grains. This method allows mimicking the high porosity of weak snow layers and reproduced a similar mixed-mode shear-compression failure envelope as observed in laboratory experiments of snow failure. The DE simulations suggest that the geometric structure of the WL as well as the tensile strength of the bonds were the most important factors influencing the failure envelope. The failure envelope obtained from the DE simulations was found to be in good qualitative agreement with experimental data for the more complex, but also more realistic weak layer type (type #3).

Furthermore, it was shown that the Mohr-Coulomb (MC) criterion is able to accurately represent the failure of a WL made of faceted crystals for loading angles higher than 20°. Hence, the MC criterion could be sufficient, in practice, to model WL failure for typical avalanche slopes that are generally steeper than 30° (Schweizer et al., 2003). In addition, the internal friction angle of the tested WL was found to be around 18° a value which is in agreement with the few previous experimental studies made on snow internal friction (Roch, 1966). However, this value is lower than the dry (or crack-face) friction which is typically around 30° (van Herwijnen and Heierli, 2009).

For slope angles lower than 20°, the shear stress sharply decreases with increasing normal stress. This phase could be simply accounted for using a modified MC cap model similarly to the Cam-Clay model or the modified Drucker-Prager cap model which has been applied for low density snow (Haehnel and Shoop, 2004).

Moreover, DE simulations of the propagation saw test were carried out for the WL of type #2. The critical length increased with increasing Young's modulus of the slab and decreased with increasing density and slope angle. An analytical model based on the extension of the deficit zone (or crack) model (Chiaia et al., 2008; Gaume et al., 2013) was then developed that also accounts for the shear stress induced by bending of the slab [Eq. (4)]. The modeled critical length was found in excellent agreement with those obtained from the DE simulations. Note that, according to Eq. (5), the trend with slab Young's modulus, which only influences the characteristic length Λ, would not change if a different type of WL would have been considered. However, the WL type would change the influence of slab density and of slope angle

since the failure criterion and thus the failure shear stress τ_p would be modified. In addition, since for snow, the Young's modulus, the density and the depth of the slab are often linked, the overall dependence of the critical length with these parameters might be more complex.

In the future, we plan to perform DE simulations of saw tests that take into account the link between the mechanical properties of the slab and compare the results with experimental data, but also consider the failure of different and more complex types of WLs. The very long-term objective, but so far unreachable due to computational issues, will be to simulate the real structure of the WL from segmented micro-tomographic images (Hagenmuller et al., 2013).

5   REFERENCES

van Baars, S. (1996). Discrete element modelling of granular materials. Heron,41(2), 139-157.

Chaudhuri, B., A. Mehrotra, F. J. Muzzio, and M. S. Tomassone (2006), Cohesive effects in powder mixing in a tumbling blender, Powder Technol., 165(2), 105–114.

Chiaia, B., P. Cornetti, and B. Frigo (2008), Triggering of dry snow slab avalanches: stress versus fracture mechanical approach, Cold Reg. Sci. Technol., 53, 170-178.

Cundall, P. A., and O. D. Strack (1979), A discrete numerical model for granular assemblies, Geotechnique, 29(1), 47–65

Delenne, J. Y., El Youssoufi, M. S., Cherblanc, F., and Bénet, J. C. (2004). Mechanical behaviour and failure of cohesive granular materials. International Journal for Numerical and Analytical Methods in Geomechanics, 28(15), 1577-1594.

Faug, T., R. Beguin, and B. Chanut (2009), Mean steady granular force on a wall overflowed by free-surface gravity-driven dense flows, Phys. Rev. E, 80(2), 021305.

Gaume, J., G. Chambon, N. Eckert, and M. Naaim (2013), Influence of weak-layer heterogeneity on snow slab avalanche release: Application to the evaluation of avalanche release depths., J. Glaciol., 59(215), 423-437.

Gaume, J., A. van Herwijnen, J. Schweizer, G. Chambon and K. Birkeland (2014), Discrete element modeling of crack propagation in weak snowpack layers. Proceedings of the International Snow Science Workshop, Banff, Canada 2014 (this issue).

Gauthier, D., and B. Jamieson, Evaluation of a prototype field test for fracture and failure propagation propensity in weak snowpack layers, Cold Reg. Sci. Technol., 51 (2), 87-97.

Hagenmuller, P., Chambon, G., Lesaffre, B., Flin, F., and Naaim, M. (2013). Energy-based binary

segmentation of snow microtomographic images. *J. Glaciol.*, *59*(217), 859-873.

Heierli, J., (2008), Anticrack Model for Slab Avalanche Release, PhD thesis, Karlsruhe University.

McClung, D. (1979), Shear fracture precipitated by strain softening as a mechanism of dry slab avalanche release, J. Geophys. Res., 84(B7), 3519-3526.

McClung, D., and J. Schweizer, Fracture toughness of dry snow slab avalanches from field measurements, J. Geophys. Res., 111, F04,008, 2006.

Nicot, F., Hadda, N., Bourrier, F., Sibille, L., & Darve, F. (2011). Failure mechanisms in granular media: a discrete element analysis. Granular Matter,13(3), 255-260.

Podolskiy, E. A., Chambon, G., Naaim, M., & Gaume, J. (2014). Evaluating snow weak-layer rupture parameters through inverse Finite Element modeling of shaking platform experiments. Nat. Hazards Earth Sys. D., 2(7), 4525-4580.

Reiweger, I., & Schweizer, J. (2013). Weak layer fracture: facets and depth hoar. The Cryosphere, 7, 1907-1925.

Roch, A. (1966). Les variations de la résistance de la neige. IAHS publication, 69, 86-99.

Rognon, P., J.-N. Roux, M. Naaim, and F. Chevoir (2008), Dense flows of cohesive granular materials, J. Fluid Mech., 596, 21–47.

Sarkar, A., and C.Wassgren (2010), Continuous blending of cohesive granular material, Chemical Engineering Science, 65(21), 5687–5698.

Schweizer, J., B. Jamieson, and M. Schneebeli (2003), Snow avalanche formation, Rev. Geophys., 41(4), 1016.

Thakur, S. C., Morrissey, J. P., Sun, J., Chen, J. F., & Ooi, J. Y. (2014). Micromechanical analysis of cohesive granular materials using the discrete element method with an adhesive elasto-plastic contact model. Granular Matter,16(3), 383-400.

Timoshenko, S.P. and J.N. Goodier (1970). Theory of Elasticity. McGraw-Hill, 608 pp.

van Herwijnen, A., and J. B. Jamieson (2005), High speed photography of fractures in weak layers, Cold Reg. Sci. Technol., 43(1-2), 71-82.

van Herwijnen, A., and Heierli, J. (2009). Measurement of crack-face friction in collapsed weak snow layers. Geophys. Res. Lett., 36(23).

van Herwijnen, A., Schweizer, J., Heierli, J. (2010). Measurement of the deformation field associated with fracture propagation in weak snowpack layers. *J. Geophys. Res., 115, F03042.*